Calculated cross sections for low energy electron collision with OH

OPEN ACCESS
IOP Publishing
Plasma Sources Science and Technology
Plasma Sources Sci. Technol. **28** (2019) 085013 (8pp)
https://doi.org/10.1088/1361-6595/ab364c

Calculated cross sections for low energy electron collision with OH

K Chakrabarti[1], **V Laporta**[2] and **Jonathan Tennyson**[3,4]

[1] Department of Mathematics, Scottish Church College, 1 & 3 Urquhart Sq., Kolkata 700006, India
[2] Istituto per la Scienza e Tecnologia dei Plasmi, Consiglio Nazionale delle Ricerche, Via Amendola 122/D, Bari, I-70126, Italy
[3] Department of Physics and Astronomy, University College London, Gower St., London WC1E 6BT, United Kingdom

E-mail: j.tennyson@ucl.ac.uk

Received 7 May 2019, revised 7 July 2019
Accepted for publication 25 July 2019
Published 19 August 2019

Abstract

The hydroxyl radical, OH, is an important component of many natural and technological plasmas but there is little available information on processes involving its collisions with low-energy electrons. Low energy electron collisions with OH are studied in the framework of the *R*-matrix method. Potential energy curves of some of the low lying target states of doublet and quartet symmetry which go to the O(^{3}P)+H(^{2}S), O(^{1}D)+H(^{2}S) and O(^{1}S)+H(^{2}S) asymptotic limits are obtained for internuclear separations between 1 and 6 a_0. Scattering calculations are performed at the OH equilibrium geometry $R_e = 1.8342\ a_0$ to yield cross sections for elastic scattering, electronic excitations from the X $^2\Pi$ ground state to the first three excited states of A $^2\Sigma^+$, a $^4\Sigma^-$, 1 $^2\Sigma^-$ symmetry and for electron impact dissociation of OH. The positions and widths for negative ion resonances in the e–OH system are used to estimate the cross section for dissociative electron attachment to OH which is found to be significant at electron energies about 1.5 eV.

Supplementary material for this article is available online

Keywords: dissociative electron attachment, electronic excitation, impact dissociation, hydroxyl radical, OH, atmospheric plasmas, combustion

1. Introduction

The hydroxyl radical, OH, is a key component of many plasmas include atmospheric ones, particularly if the air is humid [1–7] or near liquid water [8–10], and plasmas formed during combustion [11, 12]. Models of such plasmas require rates or cross sections for key processes occuring in the plasma but for OH these are largely unknown [13] and hence are absent from major data compilations [14, 15]. Indeed the best source of electron–OH rates [5] appears to be the weighted total cross-section (WTCS) calculations of Riahi *et al* [16] which, for OH, are based on old and unproven electron collision cross sections [17].

Given the difficulty in measuring electron collision cross sections with open shell species such as OH, it would appear to be timely to use theoretical methods to establish a reliable dataset of cross sections and rates for electron collisions with OH which is expected to govern its chemistry.

The starting point of our collision calculation requires accurate potential energy curves (PECs) for OH. Several studies on the PECs of OH exist. Calculations on the OH doublet and quartet states were performed as early as 1973 by Easson and Pryce [18]. Langhoff *et al* [19] studied the ground and some of the $^2\Sigma^+$ states of OH to obtain their dipole moments and radiative lifetimes. A configuration interaction (CI) study on the $^2\Sigma^-$ states of OH was performed by van

[4] Author to whom correspondence should be adressed.

Dishoeck *et al* [20]. Subsequently, they extended this work to a systematic study of the ground ($X\ ^2\Pi$) and several excited states of doublet and quartet symmetry [21]. There are also some recent and more sophisticated calculations using large GTO basis sets performed on some of the low lying OH states [22, 23].

Compared to OH, its anionic states are much less studied even though these are known to play an important role in collision processes such as the dissociative electron attachment (DEA). Singlet and triplet OH^- states of Σ^+ and Π symmetries were obtained by Sun and Freed [24] at the OH equilibrium bond length of $R_e = 1.8342\ a_0$ to calculate vertical excitation energies of the excited states of OH^-. Several calculations on the PECs of these singlet and triplet states of OH^- also exist [25–28]. More recently, calculations on the OH^- anionic states were performed with large GTO bases by Srivastava and Satyamurty [22] and Vamhindi *et al* [29]. All of the studies indicate that the $X\ ^1\Sigma^+$ state of OH^- is strongly bound whereas the $^1\Pi$ and $^3\Pi$ excited states are only quasi-bound as these resonance states lie in the continuum of the OH neutral plus free electron system.

Surprisingly few studies on electron plus OH collisions exist. A limited study of the vibrationally inelastic cross sections, both integrated and differential, for the excitation of the $\nu = 1$ vibrational level of the electronic ground state was performed by Chen and Morgan [26] in the energy range 0–3 eV using the *R*-matrix method. A much more detailed calculation of the elastic differential, integral, momentum-transfer cross sections as well as grand-total (elastic + inelastic) and total absorption cross sections for electron–OH collisions were performed by Sobrinho *et al* [30] using the Schwinger variational method and the distorted-wave approximation. Since no other results were available on *e*–OH collisions, Sobrinho *et al* compared their cross sections with the corresponding cross sections for e–H_2O collisions which they found to be remarkably similar. The ionisation potential for OH is 13 eV [31]. As mentioned above, cross section for electron impact ionisation and rate coefficients for $OH(X\ ^2\Pi) \rightarrow OH(A\ ^2\Sigma^+)$ excitations were obtained by Riahi *et al* [16] using the WTCS theory which is essentially a model calculation.

In the present work, we present cross sections and associated rates for the OH molecule for elastic scattering, electron impact electronic excitation

$$e + OH(X\ ^2\Pi) \rightarrow e + OH(A\ ^2\Pi, a\ ^4\Sigma^-, 1\ ^2\Sigma^-), \quad (1)$$

and electron impact dissociation

$$e + OH(X\ ^2\Pi) \rightarrow e + O(^3P) + H(^2S), \quad (2)$$

$$\rightarrow e + O(^1D) + H(^2S). \quad (3)$$

We also study electronic states of the OH^- negative ion and resonances in the e–OH system at the OH equilibrium bond length $R_e = 1.8342\ a_0$. Finally, an estimate of the DEA cross section

$$e^- + OH(X\ ^2\Pi) \rightarrow O^-(^2P) + H(^2S), \quad (4)$$

is made using a model proposed by Munro *et al* [32]; we are not aware of the DEA of OH being included in models of OH-containing plasmas.

The paper is organized as follows: sections 2 and 3 report the theoretical framework of *R*-matrix and the configurations for target and scattering calculations, respectively. Section 4 shows the results for PECs, couplings and cross sections. Finally, section 5 reports our conclusions and perspectives.

2. The *R*-matrix method

Our calculations are permormed using the *R*-matrix method the details of which can be found in reviews by Burke [33] and Tennyson [34]. The *R*-matrix method is based on division of the configuration space into an inner region, here a sphere of radius 11 a_0 centred at the molecular centre-of-mass, and an outer region exterior to this sphere. In the inner region, the wave function of the $(N + 1)$-electron system $(OH + e^-)$ is written as a close-coupling (CC) expansion

$$\Psi_k = \mathcal{A} \sum_{i,j} a_{i,j,k} \Phi_i(1, \ldots, N) F_{i,j}(N + 1) + \sum_i b_{i,k} \chi_i(1, \ldots, N + 1), \quad (5)$$

where $\mathcal{A}$ is the antisymmetrisation operator, Φ_i is the *N*-electron wave function of the *i*th target state, $F_{i,\ j}$ are continuum orbitals and χ_i are two-centre L^2 functions constructed by making all $(N + 1)$-electrons occupy the target molecular orbitals, and takes into account the polarization of the *N*-electron target wave function in presence of the projectile electron.

An *R*-matrix is then built at the boundary of the *R*- matrix sphere using the inner region wave function. The *R*-matrix is then propagated to asymptotic distances and matched with known asymptotic functions [35]. The matching yields the *K*-matrix from which all scattering observables can be extracted.

As Slater type orbitals (STOs) are known to provide a better target representation for diatomic targets, we used the diatomic version of the UK molecular *R*-matrix codes [36] which uses STOs to represent the target wave function. The continuum was represented by numerical orbitals in a partial wave expansion about the molecular center of mass. Since the OH target is neutral, the numerical orbitals were chosen to be spherical Bessel functions. A Buttle correction [37] was also used to allow for the arbitrary fixed boundary conditions imposed on the continuum basis orbitals.

3. Calculations

3.1. The OH target

A CI model was used to represent the OH target. As the choice of basis sets affect the quality of such calculation we tested several STO basis sets, namely those of Cade and Huo [38], Emma *et al* [39] and Langhoff *et al* [19]. Finally basis set II given in table 1 of Langhoff *et al* was chosen as it gave

Table 1. Vertical excitation energies (in eV) from the X $^2\Pi$ ground states of the OH molecule at OH equilibrium bond length $R_e = 1.8342$ a_0 . The absolute energy of the X $^2\Pi$ ground state is −75.490 110 Hartree. Also given are our computed the absolute (transition) dipole moment (μ).

OH state	This work	van Dishoeck *et al*[a]	Langhoff *et al*[b]	[22] [c]	[23] [c]	μ/D
X $^2\Pi$	0.0	0.0	0.0	0.0	0	1.60
A $^2\Sigma^+$	4.05	4.05	4.063	4.1	4.05	0.63
a $^4\Sigma^-$	7.36	6.7[d]	—	—	—	
1 $^2\Sigma^-$	7.89	7.20	—	—	—	1.45
1 $^2\Delta$	9.81	9.33	—	—	—	1.15
b $^4\Pi$	10.72	9.5[d]	—	—	—	
B $^2\Sigma^+$	10.88	10.98	11.192	—	8.75	0.94

[a] van Dishoeck *et al* [21] ($R_e = 1.85$ a_0)
[b] Langhoff *et al* [19]
[c] Estimated from the corresponding potential energy curve.
[d] Experimental adiabatic values.

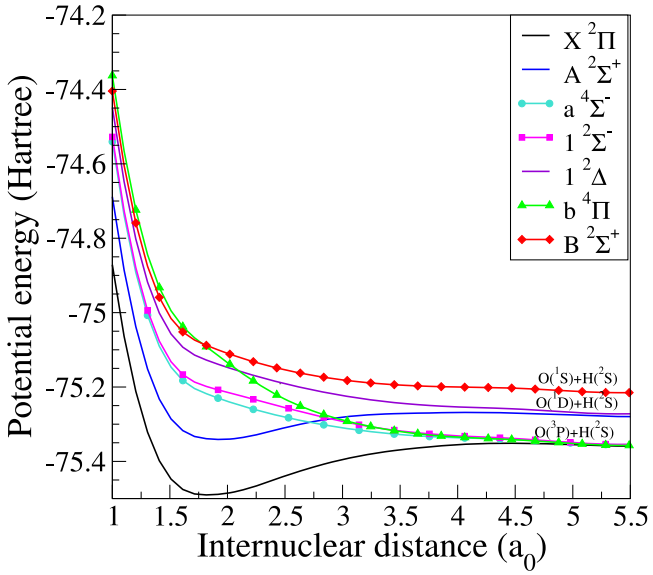

Figure 1. Potential energy curves of the first eight OH target states.

excitation energies at the OH equilibrium bond length $R_e = 1.8342$ a_0 that were in good agreement with other calculations [19, 21–23]. However, at larger bond lengths, the Langhoff *et al* basis set gave severe linear dependence in our calculation. To mitigate this, one 2*s* basis function centered on the H atom was deleted and the resulting 'trimmed' basis set was used in all subsequent calculations. This new basis set contained 10 *s*-type, 6 *p*-type, 2 *d*-type basis functions centered on the O atom and 3 *s*-type and 2 *p*-type basis functions centered on the H atom, respectively.

The STOs were used to build a basis of 35 molecular orbitals consisting of 23σ, 10π and 2δ orbitals. An initial set of SCF calculation was made for the X $^2\Pi$ and B $^2\Sigma^-$ states of OH. Two sets of natural orbitals (NOs) of $^2\Pi$ and $^2\Sigma^-$ symmetry were then obtained by doing a complete active space + singles and doubles (CAS+SD) calculation using these SCF orbitals. The NOs were then used in a subsequent CI calculation.

Tests showed that the target excitation energies were sensitive to the choice of the natural orbitals included in the CAS CI calculations. A compromise set was therefore chosen in which the 3σ, 4σ and 5σ target orbitals were represented by $^2\Sigma^-$ NOs and the remaining σ, π and δ target orbitals by $^2\Pi$ NOs.

We tested several target models. Of these, the model denoted by $(1\sigma)^2$ $(2\sigma - 6\sigma, 1\pi - 2\pi)^7$ was selected; this model has the 1σorbital frozen and the CAS was defined by $(2\sigma - 6\sigma, 1\pi - 2\pi)^7$. This model gave the best target ground state and excitation energies.

Figure 1 shows the behavior of eight lowest states of OH used in our calculation. The asymptotic limits of each of these curves are also shown in the figure. In common with previous electronic structure studies [23], we find that curves above the first excited states are repulsive.

The vertical excitation energies of some of the doublet and quartet states of OH at its equilibrium bond length, $R_e = 1.8342$ a_0, are shown in table 1. These are compared with the calculations of van Dishoeck *et al* [21] (which are more comprehensive) and those in [19, 22, 23]. The excitation energies are in good agreement with those of van Dishoeck *et al* except for the a $^4\Sigma^-$ and the b$^4\Pi$ states which are estimated form the corresponding PECs. Note also that van Dishoeck *et al* used a different value, $R_e = 1.85$ a_0 , for their equilibrium bond length. The excitation energy for the D $^2\Sigma^+$ state appears to be higher than that quoted in Qin and Zhang [23] as their value is adiabatic.

The dipole moment of the X $^2\Pi$ state was found to be 1.602 D and is in good agreement with the corresponding MCSCF value 1.612 D of Werner *et al* [40] and the measured value for the vibrational ground state of 1.655 D [41].

3.2. Scattering calculations

Our calculations are performed at a single geometry, namely the OH equilibrium geometry $R_e = 1.8342$ a_0. We have used 14 OH natural orbitals (8σ, 4π, 2δ) and a $(2 - 6\sigma, 1 - 2\pi)^7$ CAS target wave functions which allows for 2 virtual orbitals per symmetry. These were augmented by continuum orbitals F_{ij} expressed as a truncated partial wave expansion about the center of mass retaining partial waves with $l \leqslant 6$ and $m \leqslant 2$ in the expansion. Since the target was neutral, the radial parts of the continuum function was chosen to be spherical Bessel

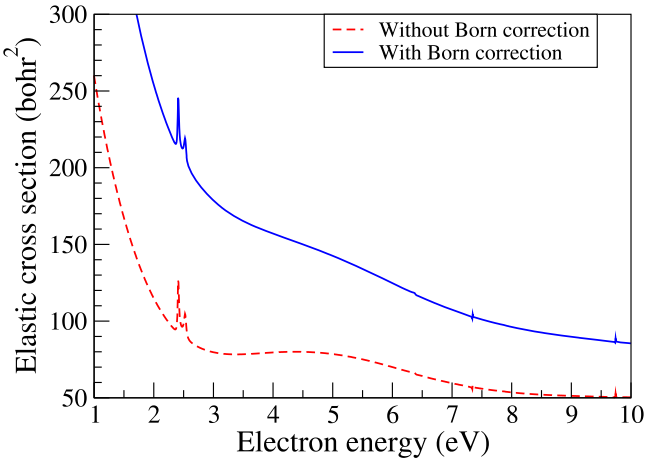

Figure 2. Elastic cross section for electron impact on OH(X $^2\Pi$) ground state at $R_e = 1.8342\ a_0$.

functions and solutions below 109 eV were retained. A Buttle [37] correction was used to correct for the effect of fixed boundary condition used to generate the functions. This produced 59σ, 49π, 40δ continuum functions which were then Schmidt orthogonalized to the target NOs.

Scattering calculations were performed on the $^1\Sigma^+$,$^1\ \Sigma^-$, $^1\Pi$,$^1\ \Delta$,$^3\ \Sigma^+$,$^3\ \Sigma^-$,$^3\ \Pi$ and $^3\Delta$ total symmetries of the e+OH system. The summary of the target states used for each symmetry in the CC expansion equation (5) is shown in table 2. Since the contribution to the cross sections from calculations of Δ symmetry were already found to be small, we did not consider higher symmetries in the calculations. Similarly we tested the effect of including higher partial waves in our continuum basis sets and found no noticeable effect once we include the Born correction discussed below.

4. Results

In the following subsections, we present our results for the OH^- bound states, resonance positions and widths at $R_e = 1.8342\ a_0$, cross sections for elastic scattering, electronic excitations and estimate of the DEA cross sections. A more complete study of the DEA process would require detailed negative ion resonance curves and widths as a function of geometry and we propose to undertake this in a subsequent paper. To the best of our knowledge, results for the cross sections presented here have never been studied before.

4.1. Bound and resonant states

The inner region solutions obtained were used to construct an *R*-matrix on the boundary. In the outer region, the potential was given by the diagonal and off-diagonal dipole moments of the OH target states. The *R*-matrices were propagated in this potential to 50 a_0 and then matched with exponentially decaying functions obtained from a Gailitis expansion [35]. To find the bound states, the searching algorithm of Sarpal *et al* [42] with the improved nonlinear, quantum defect based

Table 2. Symmetry and number of states used in the close-coupling expansion equation (5). The target states of lowest energy were used in each case.

Symmetry	Number	Target states coupled
$^1\Sigma^+$	4	One $^2\Pi$, two $^2\Sigma^+$ and one $^2\Delta$ states
$^1\Sigma^-$	3	One each of $^2\Pi$, $^2\Sigma^-$, $^2\Delta$ states
$^1\Pi$	4	One each of $^2\Pi$, $^2\Sigma^+$, $^2\Sigma^-$ and $^2\Delta$ states
$^1\Delta$	4	One each of $^2\Pi$, $^2\Sigma^+$, $^2\Sigma^-$ and $^2\Delta$ states
$^3\Sigma^+$	4	One each of $^2\Pi$, $^2\Sigma^+$, $^2\Delta$ and $^4\Pi$ states
$^3\Sigma^-$	5	One each of $^2\Pi$, $^2\Sigma^-$, $^2\Delta$,$^4\ \Pi$, and $^4\Sigma^-$ states
$^3\Pi$	5	One each of $^2\Pi$, $^2\Sigma^+$, $^2\Sigma^-$, $^4\Pi$, and $^4\Sigma^-$ states
$^3\Delta$	6	One each of $^2\Pi$, $^2\Sigma^+$, $^2\Sigma^-$, $^2\Delta$,$^4\ \Pi$, and $^4\Sigma^-$ states

Table 3. Resonance positions and widths (in eV) of some of the low lying Feshbach resonances in the e–OH at OH equilibrium bond length. $R = 1.834\ 2\ a_0$.

State	Position	Width
Below A $^2\Sigma^+$ state		
a $^3\Pi$	2.447	0.0315
A $^1\Pi$	2.536	0.0441
Below a $^4\Sigma^-$ state		
1 $^3\Sigma^+$	6.403	0.0454

grid of Rabadán and Tennyson [43] was used. This method, originally developed by Seaton [44], searches for the zeros of an energy dependent determinant $B(E)$ using either an energy or a quantum defect grid. The zeros of $B(E)$ can be shown to correspond to the bound state energies.

For resonance calculation, the *R*-matrix was propagated to 70 a_0 to obtain stable results. It was then matched with Coulomb functions using the Gailitis expansion procedure of Noble and Nesbet [35]. The recursive program RESON in the *R*-matrix code suit [45] was used to detect resonances and fit the resonances to a Breit–Wigner profile to obtain their energies (E) and width (Γ) with an initial energy grid 0.5×10^{-3} Ryd.

The resonance positions and widths of some of the low lying resonances that are relevant for DEA are shown in table 3. Interestingly, the 1 $^3\Sigma^+$ resonance is given by Vamhindi and Nsangou [29] but not by Srivastava and Satyamurthy [22], even though both these works study OH^- resonant states in some detail.

A limited number of studies on the OH^- states exist of which those of [22, 24, 26, 28, 29] are noteworthy. In particular, Chen and Morgan [26], Srivastava and Satyamurthy [22] and Vamhindi and Nsangou [29] obtained PECs for some of the OH^- states. These studies indicate that only the X$^1\Sigma^+$ state of OH^- is stable and bound. The a $^3\Pi$, A $^1\Pi$, 1 $^3\Sigma^+$ lie above the parent neutral X $^2\Pi$ state for $R \leqslant 3.0\ a_0$ and are of resonant character. However, for larger internuclear distances, these states become stable as they lie below the neutral X $^2\Pi$ state. The b $^3\Pi$ was obtained

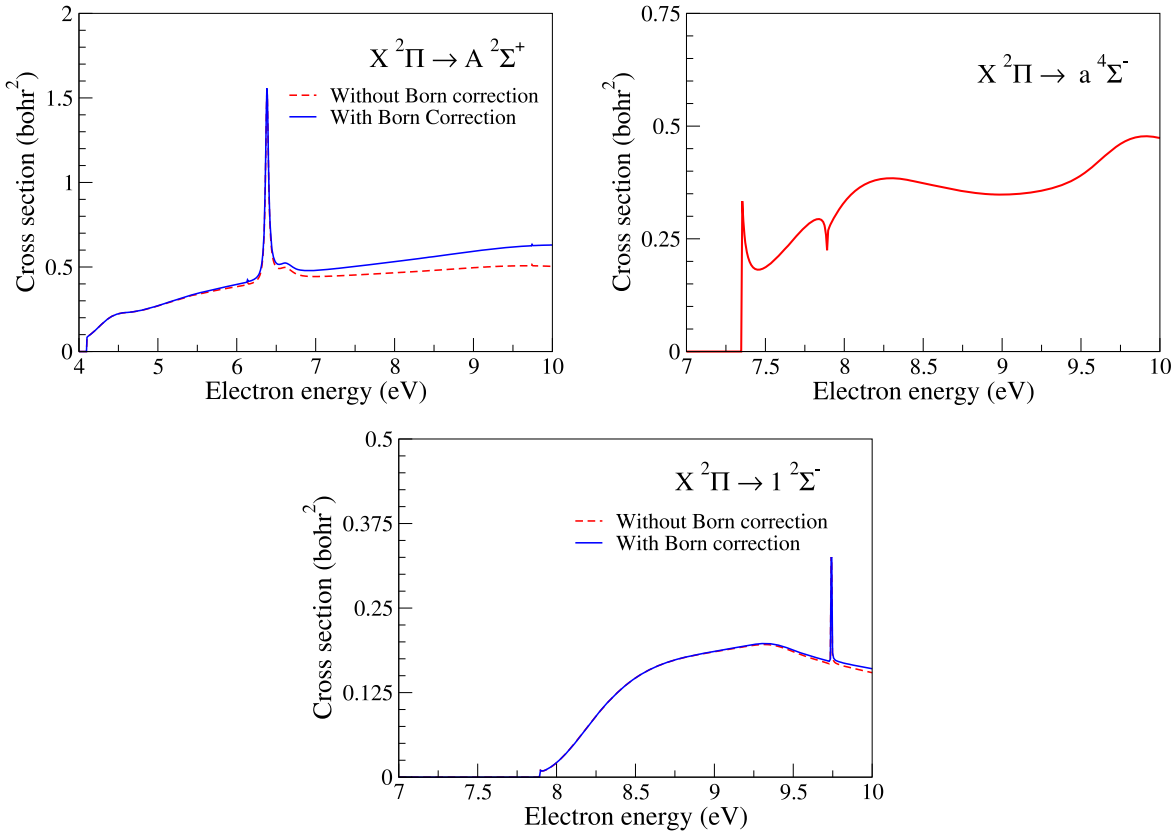

Figure 3. Excitation cross sections from the X $^2\Pi$ ground state of the OH molecule to the excited states shown in each panel for $R_e = 1.8342\ a_0$.

only by Srivastava and Satyamurthy and is of fully resonant character as it lies above the OH(X $^2\Pi$) ground state for internuclear distances R.

For a comparison of the relative positions of the $^1\Pi$ and $^3\Pi$ resonant states whose parent is OH(X $^2\Pi$), we computed the vertical excitation energies of these states and compare them with available results in table 4. Except for the corresponding results of Sun and Freed [24] which appear too high, all other results are in good agreement with each other.

Table 5 compares the energy difference ΔE between the OH(X $^2\Pi$) ground state and the X $^1\Sigma^+$, a $^3\Pi$ and A $^1\Pi$ states of OH. ΔE for the X $^1\Sigma^+$ state is the electron affinity, E_a, of OH. Our results are compared with those of Srivastava and Sharma [22], Chen and Morgan [26], Werner *et al* [40] and the experimental value of E_a given by Schulz *et al* [46]. Our values of ΔE agree reasonably with those of Srivastava and Sharma. Our computed value of the electron affinity of OH is also in close agreement with all other results, and deviates by about 0.27 eV from the experiment value [46].

4.2. Cross sections

4.2.1. Elastic scattering, electronic excitation and dissociation. Figure 2 shows cross sections for elastic scattering from OH. A Born correction to the cross sections was made to include contribution from higher partial waves. As is usual for molecules with a significant permanent dipole moment [47], the elastic cross section is strongly peaked at low energies due the strong forward scattering associated with the long-range potential due to the dipole moment. This effect is difficult to detect experimentally but has very recently been observed in low-energy collisions with water using specially designed apparatus sensitive to scattering angles of less than 3.5°[48]. The elastic cross section also features sharp peaks around 2.5 eV due to capture into the OH^- A $^1\Pi$ and a $^3\Pi$ resonant states. There is also a broad shape resonance like feature around 5 eV which may be due to temporary capture into resonant states with excited OH states as parent states.

Figure 3 shows cross sections for excitation of the OH(X $^2\Pi$) ground state to the A $^2\Sigma^+$, a $^4\Sigma^-$ and the 1 $^2\Sigma^-$

Table 4. Vertical excitation energies (in eV) from the X $^1\Sigma^+$ ground states of the OH^- molecule at the OH equilibrium bond length $R_e = 1.8342\ a_0$. Our absolute energy of the X $^1\Sigma^+$ ground state is −75.547 590 Hartree.

OH^- state	This work	Srivastava and Satyamurthy[a]	Sun and Freed[b]	Tellinghuisen *et al*
X $^1\Sigma^+$	0.0	0.0	0.0	0.0
a $^3\Pi$	3.89	3.72	9.67	3.47
A $^1\Pi$	4.01	3.93	10.62	3.75

[a] Srivastava and Satyamurthy [22]
[b] Sun and Freed [24]
[c] Tellinghuisen *et al* [28]

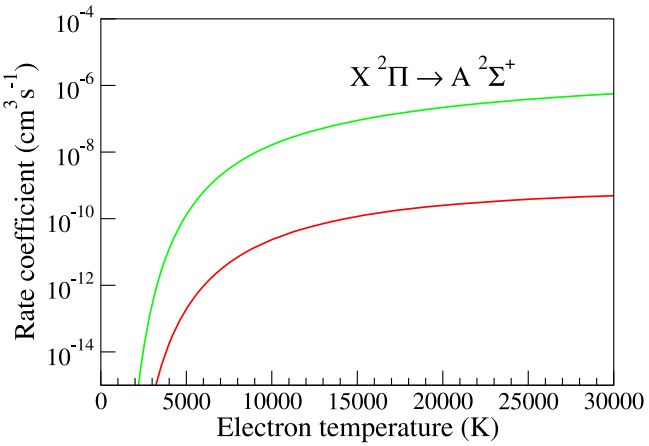

Figure 4. Rate coefficients for excitation of the X $^2\Pi$ ground state of the OH molecule to the A $^2\Sigma^+$ excited state at $R_e = 1.8342\ a_0$. Top curve Riahi *et al* [16]; bottom curve present results.

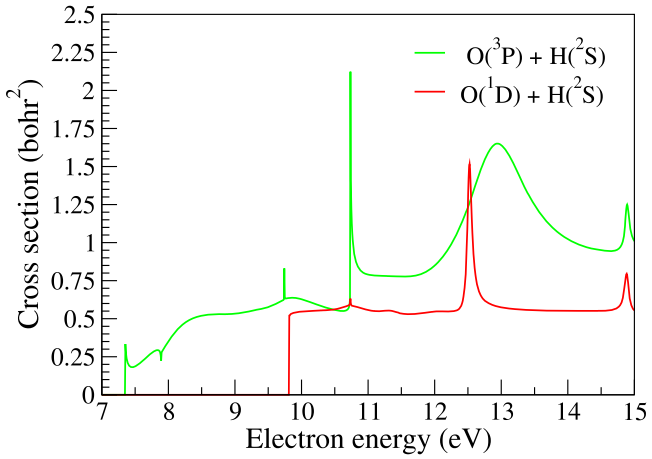

Figure 5. Cross section for electron impact dissociation of OH at $R_e = 1.8342\ a_0$ to the lowest O(^{3}P) + H(^{2}S) and to the excited O(^{1}D) + H(^{2}S) dissociation channels.

Table 5. Energy difference ΔE (in eV) between the OH(X $^2\Pi$) ground state and the X $^1\Sigma^+$, a $^3\Pi$ and A $^1\Pi$ states of the OH^- molecule at OH equilibrium bond length $R_e = 1.8342\ a_0$. ΔE for the X $^1\Sigma^+$ state is the electron affinity, E_a, of OH.

OH^- state	This work	Srivastava and Satyamurthy[a]	Chen and Morgan[b]	Werner *et al*[c]	Expt.[d]
X $^1\Sigma^+$	1.56	1.87	2.14	1.58	1.83
A $^1\Pi$	−2.53	−2.06	—	—	—
a $^3\Pi$	−2.41	−1.85	—	—	–

[a] Srivastava and Satyamurthy [22]
[b] Chen and Morgan [26]
[c] Werner *et al* [40]
[d] Schulz *et al* [46]

states. The cross sections show sharp features due to negative ion resonances. Figure 4 shows the rate coefficients for the X $^2\Pi \rightarrow$ A $^2\Sigma^+$. These are compared with the only available rate coefficients given by Riahi *et al* [16]. The rate coefficients of Riahi *et al* are obtained by fitting to an Arrhenius form $k = a\theta^b \exp(-c/\theta)$. Though the shape of the rate coefficient curves agree well, the rates given by Riahi *et al* are much larger than ours, particularly at the higher end of the temperature range. In terms of electron energy, the rates we presented are in the range 0−3 eV. In this low energy regime, the *R*-matrix method is known to give good results and hence we believe our rates to be more reliable than those of Riahi *et al*.

It is known that electron impact dissociation occurs via electronic excitation, particularly through excitation to dissociative states. OH has three repulsive dissociative states, namely the a $^4\Sigma^-$, 1 $^2\Sigma^-$ and the b $^4\Pi$ states, which go to the O(^{3}P) + H(^{2}S) asymptotic limit. Assuming that excitation to these states above the dissociation threshold ($D_0 = 3.88$ eV) results in dissociation, we present in figure 5 our estimate of the cross section for electron impact dissociation of OH. We predict that this process produces a significant quantity of excited, O(^{1}D) atoms. There appears to be no experimental or theoretical data on this process to compare with.

4.2.2. Dissociative electron attachment. To the best of our knowledge, the DEA to OH has never been studied before, theoretically or experimentally, though several works on DEA of H_2O exist [49, 50] (see also [51]). A detailed study of the DEA process would require full resonance curves and resonance widths across all internuclear distances considered and is not attempted here. However, we try to give an estimate of the DEA cross sections using an approximation developed by Munro *et al* [32].

Since the details of the method can be found in [32], we only present the essentials. The inputs for the method are the resonance positions and widths for OH^- resonances at a single geometry, here the equilibrium geometry $R_e = 1.8342\ a_0$, the PEC of the target X$^2\Pi$ ground state, and the electron affinity of OH, which is taken to be 1.56 eV from column 2 of table 5. The target PEC is chosen to be a Morse form with dissociation energy $D_e = 4.51$ eV. The A $^1\Pi$ and a $^3\Pi$ resonance potentials were chosen to be of a Morse form while the 1 $^3\Sigma^+$ resonance potential was chosen to be of an exponentially decreasing form following the shapes given by Srivastava and Satyamurthy [22] and Vamhindi and Nsangou [29] for these resonant states. We mention however, that both these works [22, 29] treat the resonant part of the A$^1\Pi$, a $^3\Pi$ and 1 $^3\Sigma^+$ potentials like bound states in their quantum chemistry calculation and hence must be treated with caution [52]. Moreover, because of their treatment of resonant states as bound, they are not able to provide the resonance widths.

Figure 6 shows our estimate of the DEA cross section. We assume that DEA produces only O^- since the singlet

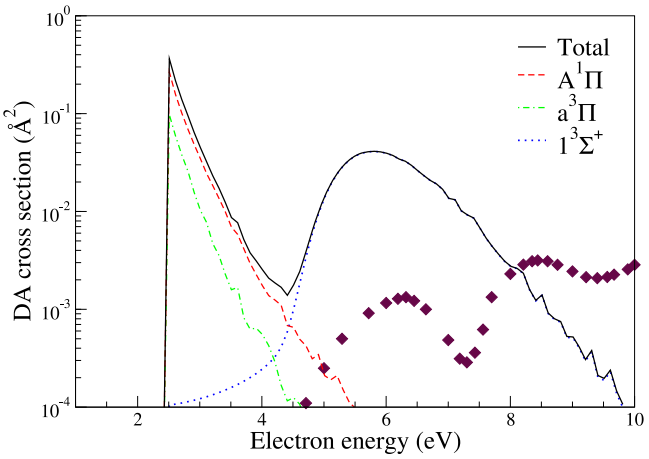

Figure 6. Cross section for dissociative electron attachment to OH for the production of O^- ions. Contributions from different resonant states are shown in dashed lines with the following convention: blue —1 $^3\Sigma^+$, green a $^3\Pi$, orange A $^1\Pi$. Filled diamonds: experimental values for O^- ion production for dissociative attachment to H_2O from table 14 of [51].

resonances cannot correlate with the $H^- + O(^3P)$ limit and all three resonance curves go asymptotically to $O^- + H(^2S)$ [22]. Since this is an approximate calculation, we are not able to comment on the details. We find a sharp peak around 3 eV which is clearly due to the A $^1\Pi$, a $^3\Pi$ resonances and a second broader peak around 6 eV which can be attributed to the 1 $^3\Sigma^+$. Since no other results are available for comparison, we have shown the experimental values [50, 51] for O^- ion production from the DEA to H_2O which also displays a similar two peak structure. We conclude therefore that the DEA process for the production of O^- ions proceeds via the A $^1\Pi$, a $^3\Pi$ resonances below 5 eV, but above 5 eV the 1 $^3\Sigma^+$ resonance mainly drives the DEA process. These cross sections are not insignificant and should be included in models of OH plasmas.

5. Conclusion

We have studied electron collision with OH using the *R*-matrix method. Scattering calculations are performed at a single geometry, namely the OH equilibrium geometry $R_e = 1.8342\ a_0$ to obtain cross sections for elastic scattering and electronic excitations to the lowest three excited states, namely the A $^2\Sigma^+$, $^4\Sigma^-$ and 1 $^2\Sigma^-$ states. We also obtained an estimate of the electron impact dissociation cross section of OH on the assumption that electronic excitation to the states going to the $O(^3P)+H(^2S)$ limit above the dissociation threshold leads to dissociation. The scattering calculations also yield OH^- bound states and negative ion resonances in the e–OH system. The X $^1\Sigma^+$ ground state of OH^- was found to be bound and several resonances that are likely to be important for DEA were identified. Since a detailed study of the DEA process is beyond the scope of this paper, an estimate of the DEA cross section was obtained using the A $^1\Pi$, a $^3\Pi$ and 1 $^3\Sigma^+$ resonances and their widths at a single geometry. To the best of our knowledge, these cross sections are being reported for the first time.

A spreadsheet containing our cross sections is provided as supplementary data, available online at stacks.iop.org/PSST/28/085013/mmedia.

Acknowledgments

VL would to thank Professor M Panesi for the kind hospitality at Aerospace Engineering Department at the University of Illinois at Urbana-Champaign (US) where this work was completed.

ORCID iDs

K Chakrabarti https://orcid.org/0000-0003-0013-5610
V Laporta https://orcid.org/0000-0003-4251-407X
Jonathan Tennyson https://orcid.org/0000-0002-4994-5238

References

[1] Benedikt J, Schroeder D, Schneider S, Willems G, Pajdarova A, Vlcek J and Schulz-von der Gathen V 2016 *Plasma Sources Sci. Technol.* **25** 045013
[2] Takeda K, Ishikawa K, Tanaka H, Sekine M and Hori M 2017 *J. Phys. D: Appl. Phys.* **50** 195202
[3] Yue Y, Pei X and Lu X 2017 *IEEE Trans. Radiat. Plasma Med. Sci.* **1** 541–9
[4] Winters C, Hung Y C, Jans E, Eckert Z, Frederickson K, Adamovich I V and Popov N 2017 *J. Phys. D: Appl. Phys.* **50** 505203
[5] Schroter S *et al* 2018 *Phys. Chem. Chem. Phys.* **20** 24263–86
[6] Wang Z, Feng C, Gao L and Ding H 2019 *J. Phys. D: Appl. Phys.* **52** 105203
[7] Shahmohammadi Beni M, Han W and Yu K N 2019 *Plasma Sci. Technol.* **21** 055403
[8] Li D, Nikiforov A, Britun N, Snyders R, Kong M G and Leys C 2016 *J. Phys. D: Appl. Phys.* **49** 455202
[9] Hsieh K C, Wandell R J, Bresch S and Locke B R 2017 *Plasma Process. Polym.* **14** e1600171
[10] Vorac J, Synek P and Hoder T 2018 *Plasma Sources Sci. Technol.* **27** 085001
[11] Ehn A *et al* 2017 *Proc. Combust. Inst.* **36** 4121–8
[12] Wang Z, Wang Y, Zhu L, Ma W, Shan J and Liu F 2019 *IEEE Access* **7** 23951–8
[13] Campbell L and Brunger M J 2016 *Intern. Rev. Phys. Chem.* **35** 297–351
[14] Pitchford L C *et al* 2017 *Plasma Proc. Polym.* **14** 1600098
[15] Tennyson J *et al* 2017 *Plasma Sources Sci. Technol.* **26** 055014
[16] Riahi R, Teulet P, Ben Lakhdar Z and Gleizes A 2006 *Eur. Phys. J.* D **40** 223–30
[17] Drawin H W 1967 Collisions and transport cross sections *Report* EUR-CEA-FC-383 Association EURATOM-C.E.A
[18] Easson I and Pryce M H L 1973 *Can. J. Phys.* **51** 518
[19] Langhoff S R, van Dishoeck E F, Wetmore R and Dalgarno A 1982 *J. Chem. Phys.* **77** 1379
[20] van Dishoeck E F, Langhoff S R and Dalgarno A 1983 *J. Chem. Phys.* **78** 4552
[21] van Dishoeck E F and Dalgarno A 1983 *J. Chem. Phys.* **79** 873

[22] Srivastava S and Sathyamurthy N 2014 *J. Phys. Chem.* A **118** 6343
[23] Qin X and Zhang S D 2014 *J. Korean Phys. Soc.* **65** 2017
[24] Sun H and Freed K F 1982 *J. Chem. Phys.* **76** 5051
[25] Komiha N, Elkaroini A and Hliwa M 1991 *J. Mol. Struct. (Theocem)* **251** 29
[26] Chen X and Morgan L A 1997 *J. Phys. B: At. Mol. Opt. Phys.* **30** 3709
[27] Nemukhin A and Grigorenko B 1997 *Chem. Phys. Lett.* **276** 171
[28] Tellinghuisen J and Ewig C S 1990 *Chem. Phys. Lett.* **165** 355
[29] Vamhindi B S D R and Nsangou M 2016 *Mol. Phys.* **114** 2204
[30] Sobrinho A M C, Lozano N B H and Lee M T 2004 *Phys. Rev.* A **70** 032717
[31] Ruscic B *et al* 2002 *J. Phys. Chem.* A **106** 2727
[32] Munro J J, Harrison S, Fujimoto M M and Tenyson J 2012 *J. Phys.: Conf. Ser.* **388** 012013
[33] Burke P G 2011 *R-Matrix Theory of Atomic Collisions* (Heidelberg: Springer)
[34] Tennyson J 2010 *Phys. Rep.* **491** 29–76
[35] Noble C J and Nesbet R K 1984 *Comput. Phys. Commun.* **33** 399–411
[36] Morgan L A, Tennyson J and Gillan C J 1998 *Comput. Phys. Commun.* **114** 120–8
[37] Buttle P J A 1967 *Phys. Rev.* **160** 719–29
[38] Cade P E and Huo W M 1967 *J. Chem. Phys.* **47** 614–48
[39] Ema I, Vega J M G D L, Ramírez G, Lopez R, Rico J F, Meissner H and Paldus J 2003 *J. Comput. Chem.* **24** 859
[40] Werner H J, Rosmus P and Reinsch E A 1983 *J. Chem. Phys.* **79** 905
[41] Peterson K I, Fraser G and Klemperer W 1984 *Can. J. Phys.* **62** 1502–7
[42] Sarpal B K, Branchett S E, Tennyson J and Morgan L A 1991 *J. Phys. B: At. Mol. Opt. Phys.* **24** 3685–99
[43] Rabadán I and Tennyson J 1996 *J. Phys. B: At. Mol. Opt. Phys.* **29** 3747–61
[44] Seaton M J 1985 *J. Phys. B: At. Mol. Opt. Phys.* **18** 2111–31
[45] Tennyson J and Noble C J 1984 *Comput. Phys. Commun.* **33** 421
[46] Schulz P A, Mead R D, Jones P L and Lineberger W C 1982 *J. Chem. Phys.* **77** 153
[47] Zhang R, Faure A and Tennyson J 2009 *Phys. Scr.* **80** 015301
[48] Kadokura R, Loreti A, Köver A, Faure A, Tennyson J and Laricchia G 2019 *Phys. Rev. Lett.* **123** 033401
[49] Compton R N and Christophorou L G 1967 *Phys. Rev.* A **154** 110
[50] Melton C E 1972 *J. Chem. Phys.* **57** 4218
[51] Itikawa Y and Mason N 2005 *J. Phys. Chem. Ref. Data* **34** 1
[52] Stibbe D T and Tennyson J 1999 *Chem. Phys. Lett.* **308** 532–6